MICROBIOLOGY

RESEARCH ARTICLE

Shuman *et al.*, *Microbiology* 2018;164:551–562

DOI 10.1099/mic.0.000646

MICROBIOLOGY SOCIETY

Transcriptome analysis of a *Pseudomonas aeruginosa sn*-glycerol-3-phosphate dehydrogenase mutant reveals a disruption in bioenergetics

Jon Shuman,[1] Tyler Xavier Giles,[1] Leslie Carroll,[1] Kenji Tabata,[2] Austin Powers,[1] Sang-Jin Suh[3] and Laura Silo-Suh[1,*]

Abstract

Pseudomonas aeruginosa causes acute and chronic human infections and is the major cause of morbidity and mortality in cystic fibrosis (CF) patients. We previously determined that the *sn*-glycerol-3-phosphate dehydrogenase encoded by *glpD* plays a larger role in *P. aeruginosa* physiology beyond its role in glycerol metabolism. To better understand the effect of a *glpD* mutation on *P. aeruginosa* physiology we compared the transcriptomes of *P. aeruginosa* strain PAO1 and the PAO1Δ*glpD* mutant using RNA-seq analysis. We determined that a null mutation of *glpD* significantly altered amino acid metabolism in *P. aeruginosa* and affected the production of intermediates that are channelled into the tricarboxylic acid cycle. Moreover, the loss of *glpD* induced a general stress response mediated by RpoS in *P. aeruginosa*. Several other phenotypes observed for the *P. aeruginosa glpD* mutant include increased persister cell formation, reduced extracellular ATP accumulation and increased heat output. Taken together, these findings implicate *sn*-glycerol-3-phosphate dehydrogenase as a key player in energy metabolism in *P. aeruginosa*.

INTRODUCTION

Pseudomonas aeruginosa can be found in a wide range of habitats and is capable of degrading a wide range of organic compounds. As an opportunistic pathogen, *P. aeruginosa* causes a wide range of serious infections in immunocompromised hosts. Within the human host, *P. aeruginosa* appears to adapt its metabolism to the available nutrients at the specific site of infection, where upregulation of specific metabolic pathways can provide a survival advantage to the bacterium [1–4]. Equally important, nutrient availability can impact on the regulation and production of virulence factors by bacterial pathogens [5]. One metabolic pathway that is highly upregulated during chronic infection of the cystic fibrosis (CF) lung, as well as acute and chronic wound infections, is glycerol assimilation [1, 6]. A better understanding of how metabolism impacts on *P. aeruginosa* physiology may lead to better therapeutic strategies to treat infections caused by this pathogen.

Glycerol-3-phosphate dehydrogenase (GlpD) is a flavin-linked enzyme that is required for glycerol catabolism in *P. aeruginosa* [7]. This enzyme oxidizes glycerol-3-phosphate to dihydroxyacetone phosphate, concurrently reducing FAD to $FADH_2$ and shuttling electrons to ubiquinone. In addition to its role in central metabolism, GlpD is also required for optimal production of several virulence determinants by *P. aeruginosa* [8]. Interestingly, *P. aeruginsoa glpD* mutants are unable to grow on glycerol as a sole carbon source in chemically defined media and are non-competitive for growth in nutrient rich media, suggesting a broader role for GlpD than its role in glycerol metabolism [9, 10].

GlpD has been implicated in persister cell formation in *Escherichia coli*, but its role in this process is controversial [11, 12]. Persister cells exist in a dormant state characterized by reduced metabolic activity, which provides protection against the harmful effects of antibiotics. Persister cells can form stochastically within a bacterial population or by selection of high-persister (hip) mutants [13, 14]. Findings by Girgis *et al.* showed that loss of *glpD* increased persister cell formation [12], while in another study the loss of *glpD* reduced persister cell formation [11]. These differences are likely due to experimental variances that are now known to impact on persister cell formation, such as inoculum age and antibiotic selection [15]. In this study we analysed the *P. aeruginosa* Δ*glpD* mutant transcriptome in order to better

Received 11 October 2017; Accepted 5 March 2018

Author affiliations: [1]Department of Basic Medical Sciences, Mercer University, School of Medicine, Macon, GA 31207, USA; [2]Daiichi University of Pharmacy, 22-1, Tamagawa-cho, Minami-ku, Fukuoka 815-8511, Japan; [3]Department of Biological Sciences, Auburn University, AL 36849, USA.
***Correspondence:** Laura Silo-Suh, silo-suh_l@mercer.edu

Keywords: *Pseudomonas aeruginosa*; transcriptome; glycerol; bioenergetics; persister cells; RpoS.

Abbreviations: ATP, adenosine triphosphate; CF, cystic fibrosis; COG, clusters of orthologous; G3P, glycerol-3-phosphate; GlpD, glycerol-3-phopshate dehydrogenase; TCA, tricarboxylic acid.

One supplementary figure and one supplementary table are available with the online version of this article.

understand how the loss of GlpD impacts on *P. aeruginosa* physiology. One important finding revealed by this study is the similarity between the *P. aeruginosa* Δ*glpD* mutant and persister cells.

METHODS

Bacterial strains, plasmids and media

The bacterial strains used in this study are listed in Table 1. PAO1 with a gentamicin cassette inserted in *glpD*, designated PAO1 *glpD*, was used for the extracellular adenosine triphosphate (ATP) and heat production experiments and was described previously [8]. A partial in-frame deletion mutant, designated PAO1 Δ*glpD*, was used for all other experiments. Unless otherwise indicated, bacteria were cultured in L-broth (LB) or on L-agar at 37 °C. Antibiotics were purchased from Sigma-Aldrich (St Louis, MO, USA) and used at the following concentrations: 100 µg gentamicin ml^{-1}, 100 µg carbenicillin ml^{-1}, 10 µg ofloxacin ml^{-1} and 800 µg kanamycin ml^{-1} for *P. aeruginosa*.

RNA isolation

Total RNA was isolated from planktonic cultures of *P. aeruginosa* PAO1 and a PAO1 Δ*glpD* mutant at an OD_{600} of ~1.8 using RiboPure (Invitrogen, Carlsbad, CA, USA). For RNA-seq analyses, three independent experiments were preformed with freshly isolated RNA from each strain. RNA sequencing was performed by the Institute for Genome Sciences, University of Maryland (Baltimore, MD, USA). After the depletion of rRNA with a commercial capture and depletion system, cDNA libraries were generated from the RNA samples. The samples were sequenced on the HiSeq 4000 sequencer, generating 150 base pair paired-end reads for each sample. An Ergatis-based [16] RNA-seq analysis pipeline was used for analysing the Illumina sequencing reads. Prior to mapping, FASTQC software (v 0.11.5) (http://www.bioinformatics.babraham.ac.uk/projects/fastqc/) was used to check the quality of the sequencing reads. Based on this information, the sequencing reads were trimmed using the FASTX-Toolkit (v 0.0.13) (http://hannonlab.cshl.edu/fastx_toolkit/index.html) to remove adapters and low-quality sequences. The sequencing reads for each RNA sample were aligned to the *P. aeruginosa* PAO1 genome using Bowtie version 0.12.9 [17]. The publicly available complete genome and annotation for *P. aeruginosa* PAO1 genome (GenBank accession no. AE004091.2) were obtained from NCBI and used for RNA-seq analysis.

HTSeq v 0.4.7 was used to determine the number of reads that aligned to annotated coding regions for each sample [18]. The DESeq R package (v 1.24.0) was used to normalize the raw counts for each sample to account for differences in library sizes and then test for differential gene expression with the negative binomial model [19]. The filter cutoffs for determining whether differences in gene expression were significant were a false discovery rate (FDR) <0.05, an absolute log fold change of ≥1 and an expression level >10th percentile. Genes were assigned to COGs for functional analysis and linked to KEGG orthologues to identify metabolic pathways [20, 21].

Real-time quantitative PCR (RT-qPCR)

Total RNA was isolated from PAO1 and the PAO1Δ*glpD* mutant as described above for the RNA-seq analyses. A half microgramme of total RNA, free of DNA, was reverse-transcribed using random hexamers and SuperScript III (Invitrogen, Carlsbad, CA, USA) to synthesize cDNA according to the manufacturer's instructions. The resulting cDNA was used as a template for RT-qPCR performed with PowerUp SYBR Green Master Mix (Thermo Fisher, Waltham, MA, USA). Three biological replicates and two technical replicates were conducted for each experiment. The primers (Table 2) were designed with Primer 3 or Primer Quest. The RNA levels were normalized to the constitutively expressed *rimM* reference gene, which encodes for the 16S rRNA-processing protein. The relative abundance of gene transcripts among the treatment groups was calculated using the 2-ΔΔ*C*t method [22].

Construction of a PAO1 Δ*glpD* in-frame deletion mutant and genetic complementation

We previously described the construction of a *glpD* in-frame deletion mutant allele and the corresponding complementing plasmid [8]. These constructs were used to generate PAO1 Δ*glpD* and the genetically complemented strain. The deletion in the *glpD* coding sequence encompasses a 351 bp fragment from nucleotide 291 to 642. *In trans* complementation was verified by PCR analysis and the complemented PAO1 Δ*glpD* strain was designated as PAO1Δ*glpD*+. The PAO1 Δ*glpD* mutant was verified for reduced pyocyanin and pyoverdine production and the complemented mutant

Table 1. Bacterial strains and plasmids

The abbreviations used for genetic markers are described by Holloway *et al.* [58]. Alternative strain names are shown in parentheses.

Strain(s) or plasmid	Genotype, relevant characteristics	Source
PAO1	Wound isolate, nonmucoid	[58]
PAO1*glpD* (LS2187)	PAO1 *glpD101*::*aacCI*	[8]
PAO1*glpD*+ (LS2251)	PAO1 *glpD* complemented for *glpD*	[8]
PAO1Δ*glpD* (LS2300)	PAO1 Δ*glpD101*	This study
PAO1Δ*glpD*+ (LS2678)	PAO1 Δ*glpD101*complemented for *glpD*	This study

Table 2. Primer sequences for RT-PCR

Gene	PA number	Forward primer sequence (5′−3′)`	Reverse primer sequence (5′−3′)
antA	PA2512	CTGGAAGCTGCAGAACGAGA	CACGGTGGCTACGTAGTTGT
catB	PA2509	CAATCTCGACGCGCATTTCG	GAAGGTGTTGCCCCTGATGT
coxB	PA0105	CCAGTGGAAGTGGCAGTACA	GCAGGTAATGCTCGTCCTTC
glpK	PA3582	CACCGATCCGTACTTCTCCG	AGGCATTGTGTAGTCGGTG
mgtA	PA4825	AATGCAGTCGCTGTTCCA	CTCTGGATGAAGGGAATCTTCTG
mmsA	PA3570	AGCAATCCCCTCGACAACAG	TCGTCGTGGTGTTCCTTGAG
pchD	PA4228	GCGTCATCGCGAGTATCTCT	GGGCAGCAGAGAGTGAAGTT
phzB1	PA4211	ACAAACTTGCGGAACATGCC	AAGAATCTTGCCGTGACCGT
phzB2	PA1900	GGAGTTGCGCAGGAAGAA	CGGTATCGGTGGTCCATAAAC
prpE	PA3568	AACTATCCCGGCTACTACCA	TGCCCGGAAACGTTTATCA
putA	PA0782	CTGGTCATCCAGGCCTACTC	CAGGCCAGGTAGGAAGTGTC
pvdA	PA2386	TTCACGATCTCATCGGTGTC	GGAGATCTGCAACTCGCTCT
rimM	PA3744	GCTGGACTATCGCCGCTG	ATCTCGTAACCGGTGAAGGTG
rpoS	PA3622	AGCAGGTTGGCGATTTCT	AGCAGGTTGGCGATTTCT
xylX	PA2518	CTTCAACAACTCCGGCAAGC	GTCGATGATCTTCGCCGACT
Hypothetical	PA4824	ACCTTCTCCGCCCTACCAT	AGGTAGAGATCCGCCGAGAG

for restoration of these phenotypes as previously described for the PAO1 *glpD* insertion mutant [8](data not shown).

Pyochelin assay

Pyochelin was assayed as described previously [23]. Briefly, *P. aeruginosa* strains were grown in L-broth to an OD_{600} of ~1.8. Three millilitres of supernatant were adjusted to pH 2.0, extracted with 1.5 mls of ethyl acetate and concentrated by rotary evaporation. The dried pellets were resuspended in methanol and chromatographed on a thin layer of silica gel G with chloroform/acetic acid/ethanol (90 : 5 : 2.5) as the mobile phase. The pyochelin spots were scraped from the plates eluted with 300 µl of methanol, evaporated and applied once more onto silica thin-layer plates for chromatography with chloroform/acetic acid/ethanol (90 : 5 : 5) as the mobile phase. Following the second thin-layer chromatography, the pyochelin spots were scraped from the plates and eluted with 130 µl of methanol, and the quantity was determined via fluorescence (excitation at 350 nm and emission at 400 nm) using black 96-well Costar plates read in a BioTek Synergy HT. At least three replicates from independent experiments were performed for each strain. A standard curve was generated using pyochelin purified using the same method as for quantitation.

Persister cell assay

To determine the number of persister cells formed, *P. aeruginosa* was grown in L-broth to an OD_{600} of ~1.8 to match the time point of the transcriptome analysis. A volume of 0.7 ml of the culture was added to an equal volume of saline and harvested by centrifugation. The pellet was then resuspended in 2 ml of L-broth and an aliquot was removed for serial dilution to enumerate the initial number of colony-forming units (c.f.u.s). To eliminate non-persister cells, the cultures were exposed to ofloxacin (10 µg ml^{-1}) and shaken at 37 °C for 5 h. The aliquots were then removed, washed and spread onto L-agar plates, and grown for at least 48 h before c.f.u. determination. The persister cells were determined by counting the number of c.f.u.s that survived antibiotic exposure and the percentage survival is reported.

Extracellular ATP quantitation

Extracellular ATP was measured using the ENLITEN ATP assay (Promega, Madison, WI, USA) as previously described [24] using strains PAO1, PAO1 *glpD* and the PAO1 *glpD* complemented strain, PAO1 *glpD*+. To monitor extracellular ATP accumulation over a growth curve, bacterial cells were inoculated into 0.4 ml of L-broth in 48-well microtitre plates and grown at 37 °C in a BioTek Synergy HT plate reader with shaking. Aliquots were taken at various time points to measure OD_{600} and extracellular ATP accumulation. Twenty-five microlitres of culture was inoculated into the wells of a white 96-flat-well polystyrene microtitre plate (Thermo Fisher), along with an equal volume of ATP reagent. The plates were then incubated for 5 min at room temperature with shaking and then read in a TECAN Infinite M1000 (Männedorf, Switzerland) using the luminescence mode and an integration time of 1000 ms. The extracellular ATP is presented as relative light units (RLU).

Glycerol-3-phosphate quantitation

Two millilitres of cells were harvested from *P. aeruginosa* cultures grown in L-broth to an OD_{600} of ~1.8. The cells were resuspended in 100 µl of glycerol-3-phosphate (G3P) assay buffer (Sigma, St Louis, MO, USA), to which 5 µl of BugBuster (EMD Millipore, Temecula, CA, USA) was added to lyse the cells. The cells were incubated for 5 min on a rotary platform and then centrifuged for 10 min at 4 °C to pellet insoluble cellular debris. G3P and protein were quantitated from the supernatants by following the assay protocols (Sigma #MAK207 and Bio-Rad's BCA protein assay reagent). In this assay, G3P is oxidized by an enzyme mix to

form an intermediate, which reduces a nearly colourless probe to a coloured product with strong absorbance at 450 nm.

Measurement of heat production using a microcalorimeter

Bacteria were grown in L-broth at 30 °C for 12 h. The turbidity of the culture was measured at 600 nm and adjusted to 0.1. To measure heat production, 10 µl of the culture medium was then inoculated on 2 ml of L-agar in a vial. The inoculated vial was then placed in a microcalorimeter (SuperCRC, Omnical Technologies, Inc., Hague, Netherlands), and the heat output from the bacterial cells in the vial was measured as previously described [25]. The heat output of bacterial cells during the exponential growth phase was determined as follows. When the amount of heat output of the vial reached approximately 0.2–0.9 µW, the vial was removed from the microcalorimeter and all bacteria in the vial were suspended in L-broth. After pelleting and washing of the bacterial cells with water, the amount of protein was determined using a DC protein assay kit (Bio-Rad, Hercules, CA, USA). The heat output was normalized to the protein concentration.

Western hybridization analysis

Protein extracts were prepared from the following *P. aeruginosa* strains grown in LB with vigorous shaking to an A_{600} of 0.5, 1.0, 1.5 and 2.0: PAO1, PAO1 Δ*glpD* and PAO1 Δ*glpD*+. The protein concentrations of the whole-cell lysates were quantified using the Bradford assay reagent (BioRad; 500–0006) and a standard curve with BSA. Approximately 30 µg per well of whole-cell lysates of protein was separated on a 7.5 % SDS-PAGE gel, along with pre-stained molecular weight standards (BioRad), and transferred to nitrocellulose for Western blotting using standard conditions. The primary antibody, anti-RpoS (rabbit poly-clonal), was used at 1 : 20 000 dilution in TBST with 1 % nonfat milk. The secondary antibody (Pierce; goat anti-rabbit conjugated HRP) was used at a dilution of 1 : 25 000. Membranes were washed 3× with TBST with 1 % milk, and once with Tris-buffered saline (TBS) prior to the addition of ECL reagent (Pierce Supersignal West Femto Max, 1 : 1; stable peroxide and luminol enhancer) for 5 min prior to visualization on X-ray film (Pierce 34091). Immediately following visualization, the blots were blocked as above, followed by a 1 : 1000 dilution of a monoclonal antibody against RNA polymerase beta subunit (Santa Cruz Biotechnology, Santa Cruz, CA, USA) in order to standardize protein loading. The secondary antibody, goat anti-mouse conjugated HRP, was used at 1 : 25 000 dilution in TBST, 1 % milk. The films were scanned using an Epson perfection V500 photo scanner in transmission mode (film, positive, 8-bit greyscale and 600 days p.i. resolution). The scan was saved as a TIFF file without compensation for background. The .tiff images were opened in Image J (https://imagej.nih.gov/ij/) and the protein bands were digitized using scanning densitometry and quantified using ImageJ version 1.51. The ratio of RpoS in the test strains relative to RpoS in the PAO1 parental strain was calculated for each A_{600} time point of the growth curve after the values had been normalized to the RpoB loading control for each specific time point (A_{600}). The dataset represents the average of at least two independent experiments. As a further control, a standard curve for RpoS was generated using serial two-fold dilutions of the PAO1 extract from the culture at an OD_{600} of 1.5 (48, 24 and 12 µg) and the RpoS protein bands were digitized and quantified as described above. The results demonstrate the reproducible quantification of a two-fold difference in signal intensity (data not shown).

RESULTS

Transcriptome changes induced by loss of GlpD function

To assess the global impact of losing the GlpD function on *P. aeruginosa* physiology, we compared the gene expression profile between PAO1 and the PAO1 Δ*glpD* mutant using next-generation RNA sequencing technology (RNA-seq). The cells for this analysis were harvested from L-broth-grown cultures at an OD_{600} of ~1.8. At this time point, which is in the late-exponential phase of growth, the *glpD* mutant grows more slowly than the parental isolate, indicating an impact on cellular physiology (Fig. S1, available in the online version of this article). Under the experimental conditions employed, the transcriptomic data revealed the expression of 352 genes that were upregulated and 254 genes that were downregulated in the Δ*glpD* mutant relative to PAO1 (Table S1). The differentially expressed genes were classified into functional categories based on clusters of orthologous gene (COG) designations. The majority of the COG function-assigned transcripts belonged to the functional categories 'metabolism' (predominant subcategories 'amino acid', 'carbohydrate' and 'lipid'), 'secondary metabolites biosynthesis, transport and catabolism', 'energy production and conversion', 'signal transduction' and 'cell wall, membrane and envelope biogenesis' (Fig. 1). Many, but not all, of these categories contained both upregulated and downregulated genes. However, upregulated genes were more numerous than downregulated genes. Unsurprisingly, the largest number of genes differentially regulated between PAO1 and the PAO1 Δ*glpD* were of either 'general function prediction only' (56 genes) and 'function unknown' (184 genes). Taken together, these findings indicate that the loss of GlpD results in a dramatically altered pattern of gene expression in *P. aeruginosa*.

Metabolic pathways are differentially regulated in the PAO1 *glpD* mutant

The most highly upregulated genes in the PAO1 Δ*glpD* mutant are involved in glycerol metabolism (Fig. 2.) and belong to the GlpR regulon (e.g. *glpKF* and *glpD*), as shown in Table S1. This was an expected result, because disruption of *glpD* results in increased intracellular concentration of glycerol-3-phosphate (G3P) in *E. coli*, which is the inducer for the GlpR regulon [11, 26]. Consistent with these findings, we determined that the Δ*glpD* mutant accumulates

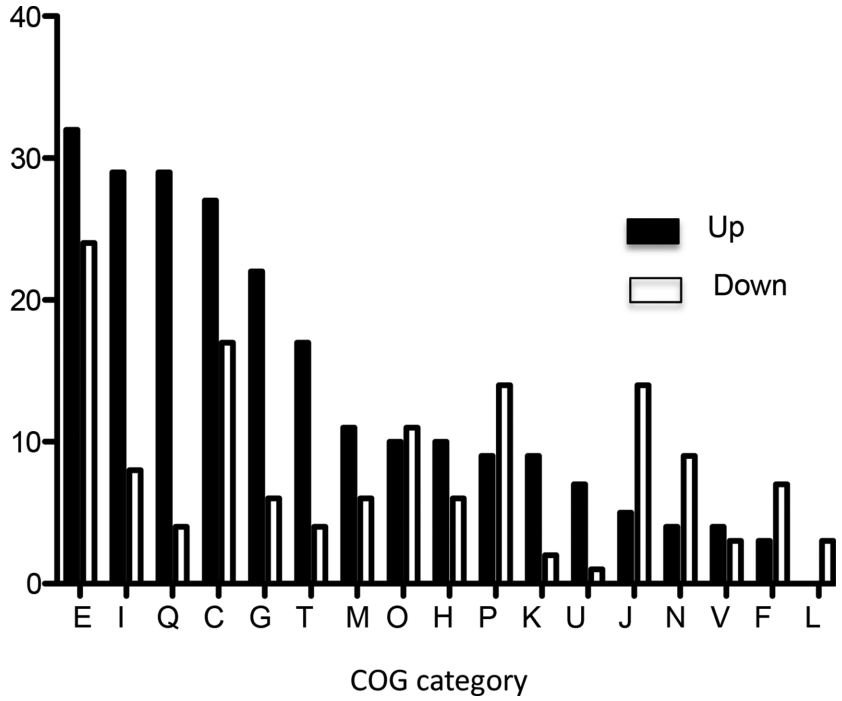

Fig. 1. Cluster of orthologous groups (COG) functional categories. Functional classification of the genes upregulated and downregulated by a deletion in *glpD*. COG category descriptions: E, amino acid metabolism and transport; I, lipid metabolism; Q, secondary metabolites, biosynthesis and transport catabolism; C, energy production and conversion; G, carbohydrate metabolism and transport; T, signal transduction; M, cell wall/membrane/ envelope biogenesis; O, post-translational modification, protein turnover and chaperone function; H, coenzyme transport and metabolism; P, inorganic ion transport and metabolism; K, transcription; U, intracellular trafficking, secretion and vesicular transport; J, translation, ribosomal structure and biogenesis; N, cell motility; V, defence mechanisms; F, nucleotide transport and metabolism; L, replication, recombination and repair.

G3P and that complementation of the mutant with a wild-type copy of the gene restores extracellular G3P accumulation to wild-type levels (Table 4). G3P accumulation in the Δ*glpD* mutant in the absence of exogenous glycerol as a carbon source is largely attributed to the activity of the biosynthetic glycerol-3-phosphate dehydrogenase encoded by *gpsA*.

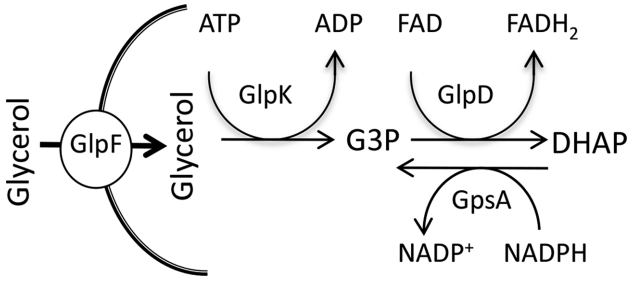

Fig. 2. Glycerol metabolism in *P. aeruginosa*. Glycerol transport into *P. aeruginosa* cells is facilitated by GlpF (glycerol facilitator). Intracellular glycerol is converted to glycerol-3-phosphate (G3P) in an ATP-requiring phosphorylation reaction catalyzed by glycerol kinase encoded by *glpK*. *sn*-glycerol-3-phosphate dehydrogenase, encoded by *glpD*, oxidizes glycerol-3-phosphate to dihydroxyacetone phosphate (DHAP), concurrently reducing FAD to $FADH_2$. Biosynthetic glycerol-3-phosphate dehydrogenase (GpsA) is a cytoplasmic protein that converts DHAP to G3P.

The next most highly upregulated group of genes in the Δ*glpD* mutant are involved in tryptophan metabolism, including the anthranilate and ketoadipate pathway genes (Fig. 3 and Table 3). The ultimate end products of these combined pathways are succinyl-CoA and acetyl-CoA, which are key intermediates in energy generation through the tricarboxylic acid cycle. Anthranilate can also serve as an intermediate in pyocyanin and *Pseudomonas* quinolone signal (PQS) biosynthesis. Pyocyanin is a redox-active secondary metabolite that has broad inhibitory activity against other microbial organisms, while PQS is a cell–cell communication molecule that regulates a variety of virulence genes in *P. aeruginosa*. Interestingly, the transciptome results support the routing of anthranilate into pyocyanin and not PQS production (Fig. 3 and Table 3). Both of the *phz* operons that encode for enzymes involved in the synthesis of phenazine-1-carboxylic acid (PCA) were upregulated in the PAO1 Δ*glpD* mutant. In addition, the genes involved in the conversion of PCA to either pyocyanin (*phzM* and *phzS*) or phenazine-1-carboxamide (*phzH*) were also upregulated in

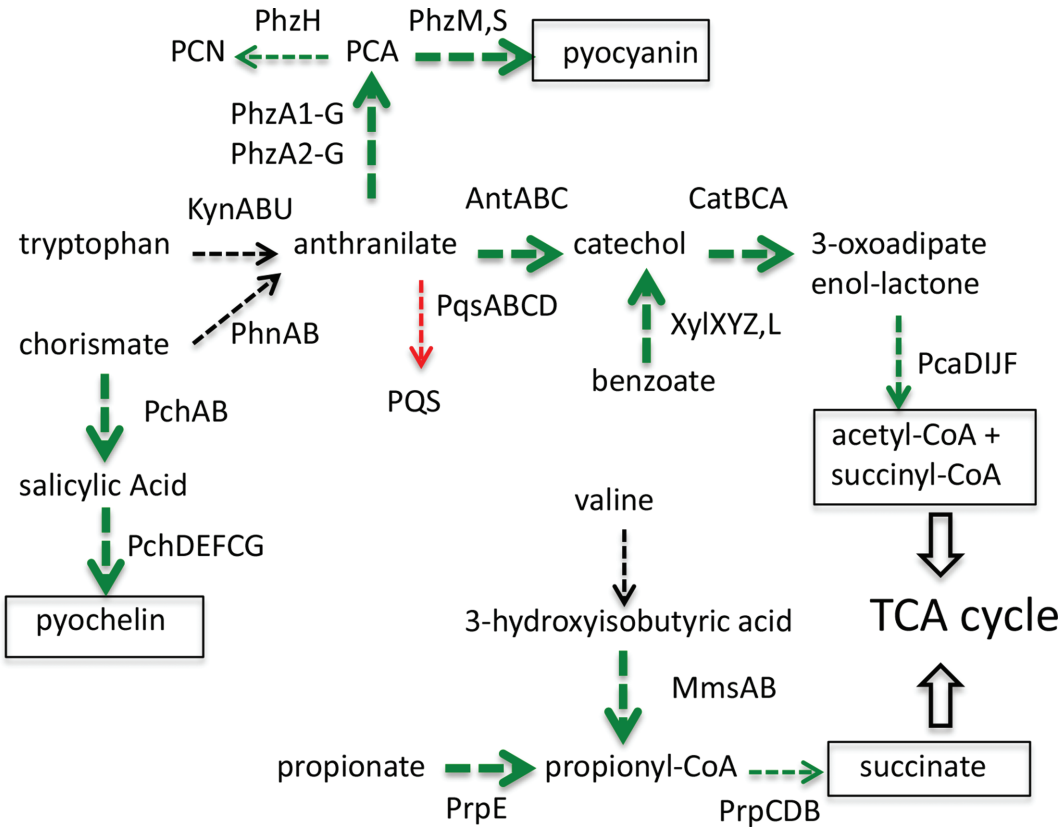

Fig. 3. Main metabolic pathways affected by the deletion of *glpD*. Green arrows indicate upregulated pathways and red arrows indicate downregulated pathways, with the thickness of the arrow indicating the relative strength of regulation. Black arrows indicate pathways not affected or not tested. PCN, phenazine-1-carboxamide; PCA, phenzine-1-carboxylic acid; TCA, tricarboxylic acid. Boxes indicate key metabolites.

the Δ*glpD* mutant. In agreement with these results is the upregulation of *opmD,* which is a component of an efflux pump that transports phenazines (Table S1). These findings contradict our previous results, which showed pyocyanin production was reduced in the Δ*glpD* mutant compared to the parent strain, PAO1 (8). However, the RNA-seq analysis was conducted on an late-exponentially growing population, while pyocyanin production was measured using late-stationary-phase cells. To clarify this difference, we investigated *phzB1* expression in late-stationary-phase cells by RT-qPCR and determined that *phzB1* expression is reduced approximately by twofold in the PAO1 Δ*glpD* mutant compared to the parent strain at this time point (data not shown). Therefore, *phzB1* expression is unusually high during exponential growth in the PAO1 Δ*glpD* mutant, but drops below PAO1 levels in the late-stationary phase of growth.

Either chorismate or tryptophan may serve as the substrate for anthranilate. However, chorismate appears to be directed towards the production of pyochelin, as indicated by upregulation of the *pch* genes in this pathway in the Δ*glpD* mutant (Table 3 and Fig. 3). Pyochelin is one of two siderophores produced by *P. aeruginosa* that functions in iron assimilation. Normally, siderophores are produced in response to iron-limiting conditions and not under the rich media conditions used here for the RNA-seq analysis. To verify the upregulation of pyochelin production in the PAO1 ΔglpD mutant, we quantitated the production of this siderophore under the same growth conditions as were used for the RNA-seq analysis. As shown in Table 4, the pyochelin levels were barely detectable in the PAO1 cultures, but were highly elevated in the PAO1 ΔglpD mutant, which corroborates the RNA-seq results. Further, expression of the biosynthetic genes (*pvd*), which encode for pyoverdine, the second siderophore produced by *P. aeruginosa*, was downregulated in the Δ*glpD* mutant according to RNA-seq, which supports the findings of our earlier study, which showed PAO1*glpD* is reduced for pyoverdine production (Table 3) [8].

Another significantly upregulated set of genes in PAO1 Δ*glpD* leads to the production of succinate from propionyl-CoA (Table 3 and Fig. 3). The *mmsAB* operon encodes for 3-hydroxyisobutyrate dehydrogenase and methylmalonate-semialdehyde dehydrogenase, respectively, and these

Table 3. Selected genes that are differentially regulated between PAO1 and PAO1Δ*glpD* by RNA-seq

Genes are clustered according to metabolic or biosynthetic pathway and the values shown are the maximum fold change of genes in the cluster rounded up to the nearest decimal. A positive value indicates an increased expression in PAO1Δ*glpD* compared to the wild-type PAO1. ND, not determined. The corresponding *P*-values for the log fold changes are shown.

PA number	Gene	Function	Log_2 FC	*P*-value
PA3581-82	*glpFK*	Glycerol metabolism	6.69	4.5e–52
PA3584	*glpD*			
PA2512-2514	*antABC*	Anthranilate metabolism	5.4	5.7e–41
PA3569-3570	*mmsAB*	Valine catabolsim	5.53	3.7e–40
PA2507-2509	*catBCA*	Catechol metabolsim	4.01	2.2e–09
PA2515-2518	*xylXYZL*	Benzoate metabolism	4.3	1.8e–23
PA1899	*phzA2*	Phenazine biosynthesis	3.68	1.0e–22
PA1900-1905	*phzB2-G2*			
PA4210	*phzA1*		2.97	
PA4211-4216	*phzB1-G1*	Phenazine biosynthesis		1.8e–15
PA4209	*phzM*			
PA4217	*phzS*			
PA0105-0108	*coxAB, coIII*	Cytochrome c oxidase	2.83	3.4e–15
PA4224-4226	*pchGFE*	Pyochelin biosynthesis	2.73	1.2e–13
PA4228-4231	*pchABCD*			
PA3568	*prpE*	Propionyl-CoA metabolism	3.48	1.6e–20
PA0795-0798	*prpBC*			
PA0792	*prpD*			
PA0996-0999	*pqsABCD*	Quinolone synthesis	−1.4	2.6e–05
PA2386	*pvdA*	Pyoverdine biosynthesis	−1.67	4.4e–06
PA2396	*pvdF*			
PA2425-2426	*pvdGL*			
PA2394-95	*pvdNO*			
PA0782	*putA*	Proline dehydrogenase	−4.27	4.7e–26
PA4824	ND	Hypothetical	−5.38	1.8–34

enzymes function in the distal pathway of valine degradation. The *mmsAB* operon is positively regulated by the transcriptional regulator MmsR [27]. However, no changes in *mmsR* expression in the Δ*glpD* mutant were identified by the transcriptome analysis. Taken together, both the anthranilate and valine pathways of assimilation are highly upregulated in the PAO1 Δ*glpD* mutant compared to PAO1, indicating significant alterations in amino acid metabolism and the production of intermediates for the tricarboxylic acid (TCA) cycle.

Table 4. Effect of a *glpD* deletion on G3P and pyochelin accumulationGlycerol 3-phosphate (G3P) and pyochelin accumulation by PAO1, PAO1 Δ*glpD* and the complemented mutant (PAO1 Δ*glpD*+) are shown. The results presented are the average of three independent experiments with standard deviations.

Strain	G3P nm mg^{-1} protein	Pyochelin (μg ml^{-1})
PAO1	0.0206 (±0.01)	0.08±0.15
PAO1Δ*glpD*	0.4343 (±0.13)	7.27±0.38
PAO1Δ*glpD*+	0.0389 (±0.09)	1.58±0.35

Stress-response genes are induced by deletion of *glpD*

The upregulation of the genes involved in stress response in the Δ*glpD* mutant represents another major finding of the transcriptome analysis. The genes upregulated in the PAO1Δ*glpD* mutant that are associated with an oxidative stress response include *napF*, *pchR*, *fptA*, *PA1951, PA4219* and *osmC*. In addition, the genes associated with an envelope stress response were also upregulated in PAO1 Δ*glpD* and include *lptF*, *fusA2*, *PA1323, PA2562*, *PA2815, PA3460* and *PA3691*. However, the largest group of stress-response genes upregulated in the Δ*glpD* mutant belongs to the general stress-response regulon mediated by the alternative sigma factor, RpoS. Approximately 35 % of the genes upregulated in the Δ*glpD* mutant are also regulated by RpoS (Table S1). The RT-qPCR results supported the upregulation of *rpoS* expression (Fig. 4). However, RpoS can be regulated at several levels beyond the level of transcription initiation [28]. Subsequently, we determined by Western blot analysis that RpoS is approximately threefold more abundant in the Δ*glpD* mutant compared to the parental strain during exponential growth (Fig. 5).

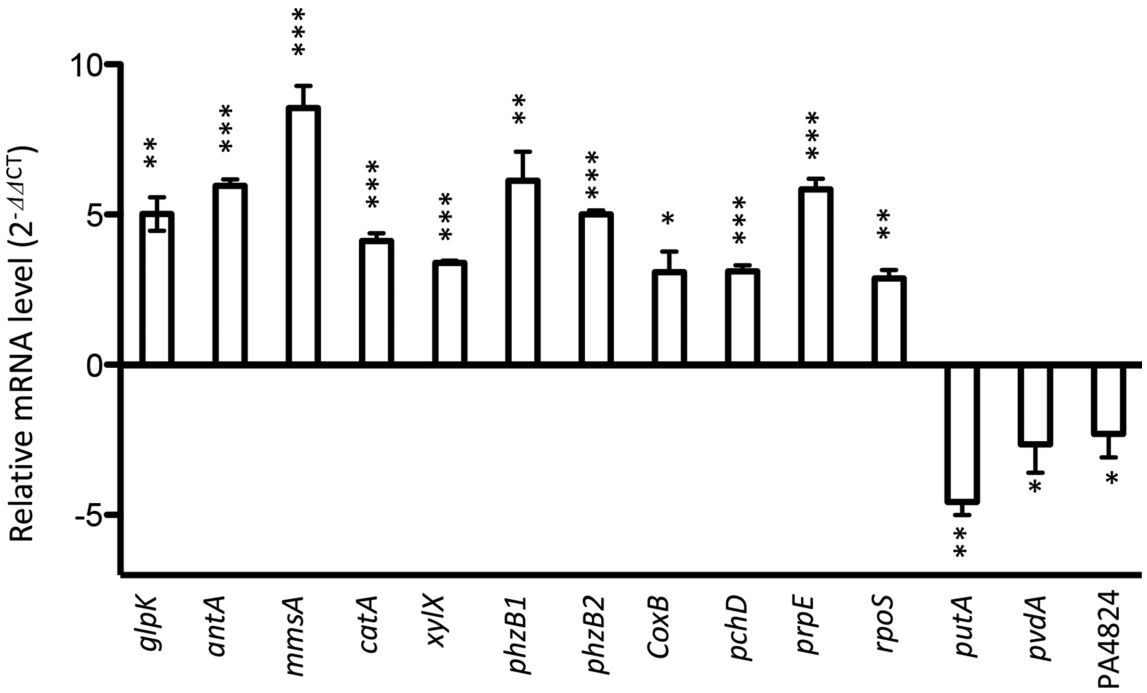

Fig. 4. RT-qPCR verification. Real-time quantitative reverse transcription (RT-qPCR) analysis of target gene expression in PAO1 ΔglpD compared to PAO1. Normalization using expression of the *rimS* gene was performed using the 2-ΔΔCt method. *, ** and *** indicate $P<0.05$, $P<0.001$ and $P<0.0001$, respectively.

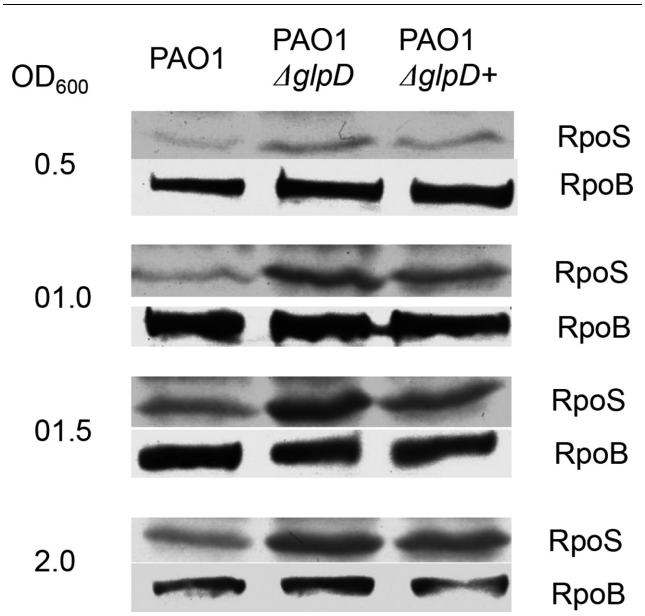

Fig. 5. Western blot analysis of RpoS. Bacterial protein extracts were electrophoresed on SDS-polyacrylamide gels, blotted onto nitrocellulose and probed with a polyclonal antibody against RpoS. Samples were collected at $OD_{600\,nm}$ values of 0.5, 1.0, 1.5 and 2.0. RpoB was used as a loading control and probed with anti-RpoB antibody.

One of the RpoS targets significantly upregulated in the Δ*glpD* mutant is the operon encoding for the aa3-type cytochrome c oxidase. This particular cytochrome c is highly efficient for generating a proton gradient and expression of the operon is induced under conditions of starvation for carbon, nitrogen or iron [29, 30]. Consequently, upregulation of this operon suggests that the Δ*glpD* mutant may perceive a starvation situation. Altogether, our results indicate that the loss of GlpD function leads to increased RpoS and induction of the RpoS regulon in *P. aeruginosa*.

Genes downregulated in the Δ*glpD* mutant

Unlike the genes that are upregulated in the PAO1Δ*glpD* mutant, the downregulated genes do not suggest an obvious unifying theme. Some of the downregulated genes may support metabolic stasis and others may play a protective role. One of the most highly downregulated operons in PAO1 Δ*glpD* is associated with polyamine synthesis (PA5506–PA5509). Polyamines have diverse functions in bacteria and reduced production of these molecules is associated with reduced growth in some bacteria [31, 32].

Several of the genes downregulated in the Δ*glpD* mutant appear to play a protective role in cellular metabolism and bioenergetics. One such gene is *mgtC* (PA4635), which encodes for an inhibitor of the F_1F_O ATP synthase. Downregulation of this gene in the Δ*glpD* mutant should help to conserve ATP levels [33]. The genes encoding for proline dehydrogenase, *putA*, and the proline symporter, *putP*, were

also downregulated in the Δ*glpD* mutant. Proline oxidative metabolism generates reactive oxygen species (ROS) in mitochondria and in *E. coli*, suggesting that downregulation of these genes may be protective [34, 35]. Reduced proline metabolism may also result in the internal accumulation of proline, which has been shown to have a variety of protective effects for the cell, including acting as an important osmolyte against osmotic stress.

Quantitative RT-PCR verification

To confirm the changes in the expression observed with the transcriptome analysis, we investigated the expression of select upregulated and downregulated genes by RT-qPCR analysis. As shown in Fig. 4, the direction and level of gene expression between PAO1 and PAO1 Δ*glpD* agreed well between the two techniques.

Loss of GlpD function results in increased persister cell formation

The metabolic rearrangements that accompany the loss of GlpD function mirror several characteristics of persister cells, including the induction of alternative metabolic pathways leading into the TCA cycle and the induction of the RpoS regulon [36, 37]. These similarities prompted an investigation into persister cell formation by the PAO1 Δ*glpD* mutant. For this experiment, we grew *P. aeruginosa* to an OD_{600} of ~1.8 before exposing the cells to ofloxacin. At this growth point, induction of the RpoS regulon and the accompanying metabolic rearrangements are both in effect in the Δ*glpD* mutant. As shown in Fig. 6, the Δ*glpD* mutant is significantly increased for persister cell formation compared to the wild-type, while the complemented mutant is restored for wild-type frequency. Taken together, the results suggest that the altered metabolic changes and/or RpoS induction play a role in persister cell formation in this mutant.

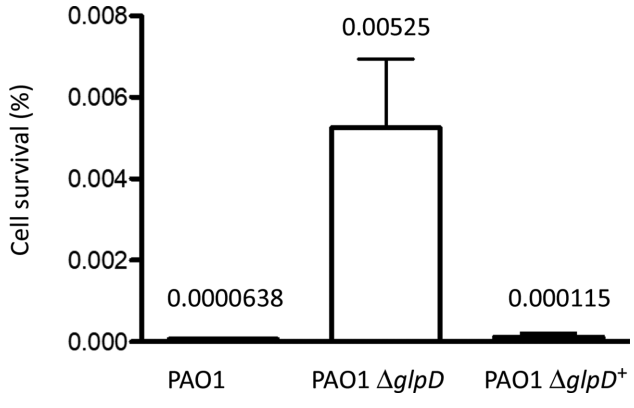

Fig. 6. Effect of a *glpD* deletion on persister cell formation. Bacterial cells in the logarithmic phase of growth were exposed to ofloxacin (10 μg ml^{-1}) for 5 h at 37 °C. The percentage of cells surviving antibiotic exposure was determined from plate counts. The values presented are averages of six independent experiments, with the error bars indicating standard deviation.

The *glpD* mutant is reduced for extracellular ATP accumulation and increased for heat production

Compromised bioenergetics may be an important aspect of the persister phenotype, as indicated by several studies that either characterized persister mutants or artificially induced a persister state [38, 39]. We therefore tested whether bioenergetics was affected by the loss of GlpD in *P. aeruginosa*. We had determined previously that extracellular ATP correlates with bacterial metabolism and is reduced in bioenergetic mutants of *P. aeruginosa* [24]. As shown in Fig. 7(a), the PAO1*glpD* insertion mutant is reduced for extracellular ATP throughout the growth cycle, while complementation

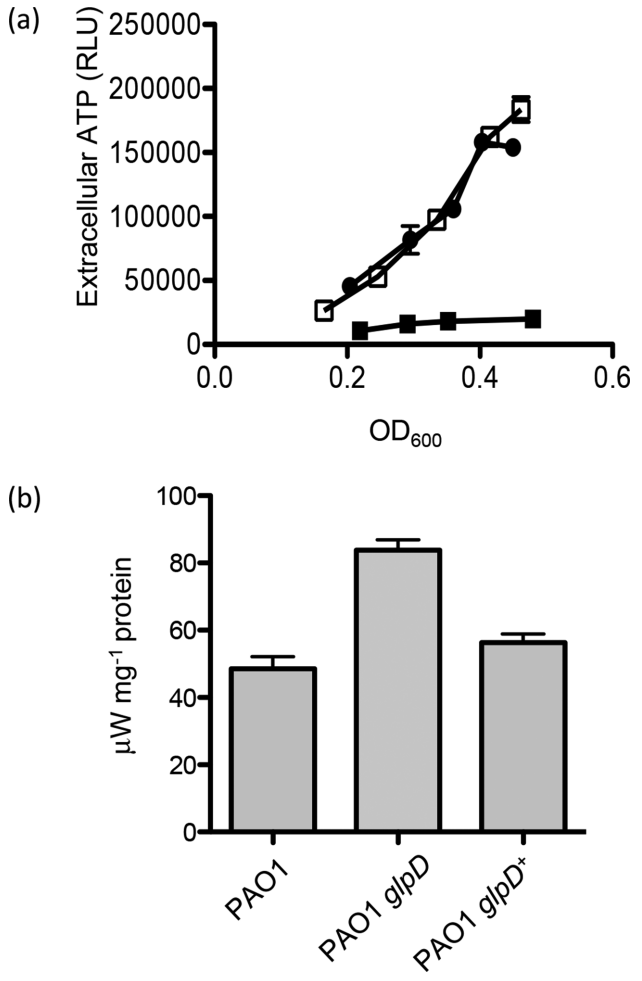

Fig. 7. The *glpD* mutant is reduced for extracellular ATP accumulation and increased for heat output. (a) Extracellular ATP accumulation. Closed circles represent the parent (PAO1), closed squares represent the PAO1*glpD* mutant and open squares represent the complemented strain (PAO1*glpD*+). Extracellular ATP is presented as relative light units (RLU). The values are the mean±SE of triplicate measurements and are representative of two experiments. (b) Heat output by *P. aeruginosa*. The heat production of *P. aeruginosa* grown on L-broth was measured using a microcalorimeter. The heat output was normalized to the protein concentration. The values were determined from three replicates and are presented as the mean±SD.

with a wild-type copy of the gene restored extracellular ATP accumulation to wild-type levels. Taken together, the results suggest that the loss of GlpD compromises the bacterium's ability to generate ATP. Interestingly, RpoS proteolysis appears to be regulated by ATP levels in *E. coli* [40]. Therefore, the induction of the RpoS regulon in the Δ*glpD* mutant may be a consequence of reduced ATP pools.

We next compared the heat output of PAO1, PAO1 *glpD* and the PAO1 *glpD*+ strains to better understand the mechanistic basis for reduced ATP pools. Heat production by bacteria is tightly coupled to metabolism, but it is also an indication of energy-spilling reactions [25, 41–43]. Energy-spilling reactions (also called uncoupling reactions) produce heat from metabolism instead of channelling metabolic yield into ATP synthesis. As shown in Fig. 7(b), heat output was significantly increased in the *glpD* mutant compared to the wild-type and the complemented strain suggesting uncoupling of oxidative phosphorylation from ATP synthesis. The results suggest that more energy is directed towards heat production in the PAO1 *glpD* mutant compared to PAO1.

DISCUSSION

This comparative transcriptome analysis generated a novel dataset describing the functional response of *P. aeruginosa* to the loss of glycerol-3-phosphate dehydrogenase. Our results reveal that the loss of GlpD function induces a robust response in genes related to anthranilate metabolism and the RpoS-mediated general stress response.

The observed metabolic alterations reflect a shift of available resources to altered carbon flow through the TCA cycle. However, some of the energy generated from this metabolic shift appears to be lost to heat production rather than into ATP synthesis or biomass production. We suspect that these disruptive perturbations are the inducer for the RpoS-mediated general stress response in the *glpD* mutant. It is important to note that metabolic perturbances can increase RpoS levels, which have been associated with decreased specific growth rates in *E. coli* [44–46]. In addition, our results are consistent with another study that shows a direct relationship between ATP levels and RpoS proteolysis [40]. Normally, low RpoS levels are observed in bacteria during exponential growth due to high ATP levels. ATP powers the protease ClpXP, which degrades RpoS. As bacterial cells enter the stationary phase, ATP levels decline and RpoS is stabilized as ClpXP activity diminishes. Our results indicate that RpoS levels are elevated during exponential growth in the *P. aeruginosa glpD* mutant, which is likely due to reduced ATP levels.

Interestingly, some of the physiological changes induced in the *glpD* mutant share a strong resemblance to persister cell physiology. These include altered amino acid metabolism, altered carbon flow to the TCA cycle, induction of the RpoS stress response and reduced accumulation of ATP [36, 37, 47, 48]. A recent study showed that the point at which carbon flows into the TCA cycle affects the PMF generated and subsequently the persister cell state in *P. aeruginosa* [49]. Obviously, bypassing oxidation reactions in the TCA cycle involved in NADH production has a negative effect on energy generation. Our study suggests that succinate is the point at which much of the carbon flows into the TCA cycle in the *P. aeruginosa glpD* mutant. This process would bypass two oxidation steps for NADH production in the TCA cycle and thereby affect respiration.

The role of RpoS in persister cell formation in *E. coli* and *P. aeruginosa* is unclear based on the differential results obtained by several studies. Deletion of *rpoS* dramatically increased persister cell formation in *E. coli* [50], leading the authors to propose that an impaired stress response results in amplified persister cell formation. However, another study showed that *E. coli rpoS* mutants may be increased or decreased for persister cell formation, depending upon the antibiotic used to kill non-persister cells [51]. Similarly, *P. aeruginosa rpoS* mutants can be increased or decreased for persister cell formation, depending upon growth conditions and antibiotic selection [50, 52, 53]. Our results indicate that RpoS is upregulated in the PAO1*glpD* mutant, which results in induction of the RpoS regulon. However, more detailed studies will be needed in order to determine whether induction of the RpoS regulon contributes to, or limits, persister cell formation in *P. aeruginosa*. Finally, a very recent publication showed that lowering ATP levels in *E. coli* leads to persister cell formation by decreasing the activity of antibiotic targets [48]. Therefore, reduced ATP is becoming a hallmark of persister cell physiology. Historically, persister cells have been considered to be in a state of dormancy based on the lack of killing by antibiotics that target growing cells [54]. More recently it has been recognized that reduced metabolic activity in bacteria increases the probability of entering the persister state, although it is not an absolute requirement [36].

Our study suggests that the uncoupling of electron transport from ATP synthesis may play a role in persister cell formation. The mechanisms that dissipate the proton motive force have been shown to induce persister cell formation in bacteria. For example, induction of the toxin–antitoxin component TisB toxin increases persister cell formation in *E. coli* by dissipation of the proton motive force [39]. Likewise, treatment with carbonyl cyanide *m*-chlorophenylhydrazone (CCCP), an uncoupler of oxidative phosphorylation, also induces the persister state in *E. coli* [38].

Interestingly, our study suggests a similarity in the function of GlpD for bacteria and mammalian cells. Specifically, transgenic mice that lack mitochondrial glycerol-3-phosphate dehydrogenase (mGPD) show increased expression of uncoupling protein 3 [55]. Uncoupling proteins allow protons to enter the mitochondrial matrix in a process that bypasses ATP synthase, leading to a reduction in energy efficiency and the generation of heat [56]. We suspect other similarities may exist in the function of GlpD across evolutionary lines and we are particularly interested in the role of mGPD in redox cycling via the glycerol phosphate shuttle

[57]. It will be important to determine whether this function is conserved in bacterial GlpD.

Our expression data provides new information about the physiological status of *P. aeruginosa* upon the loss of GlpD function and provides an explanation for the pleitropic effect of the mutation. GlpD functions at the nexus of respiration, central carbon metabolism and phospholipid biosynthesis. Consequently, the deletion of *glpD* is expected to impact on bioenergetics through several different mechanisms. First, during catalysis GlpD shuttles electrons into the electron transport chain by reducing ubiquinone. Therefore, diminished flow of electrons upon the loss of GlpD is consistent with the observed decrease in ATP levels and the concomitant induction of the RpoS regulon and the alternative aa3-type cytochrome c oxidase. Second, GpsA, which catalyzes the reduction of DHAP to G3P with consumption of NADH, may siphon DHAP away from the Entner–Doudoroff pathway. This diversion of carbon substrates is consistent with the observed reduction of alginate and rhamnolipid accumulation previously noted for the *P. aeruginosa glpD* mutant [8]. These alterations would also diminish ATP production. Third, induction of the pathways for assimilating tryptophan and valine to produce substrates that bypass two oxidative decarboxylation steps in the TCA cycle would have a negative impact on ATP synthesis. Finally, wasteful dissipation of the proton motive force through increased heat production would contribute to a reduction in ATP synthesis. In summary, the disruption of bioenergetics caused by the loss of GlpD affects a large range of phenotypes and processes.

Funding information
This research was supported by funds from a Mercer University SEED grant [to L. A .S (#26609) and J. S. (#226911)], from a Mercer University and MEDCEN Community Health Foundation award (#570196/570197 to L. A. S.) and from the Hatch program of the USDA-NIFA (#ALAOSUH to S. -J. S.).

Conflicts of interest
The authors declare that there are no conflicts of interest.

References

1. Turner KH, Everett J, Trivedi U, Rumbaugh KP, Whiteley M. Requirements for *Pseudomonas aeruginosa* acute burn and chronic surgical wound infection. *PLoS Genet* 2014;10:e1004518.
2. Berger A, Dohnt K, Tielen P, Jahn D, Becker J *et al.* Robustness and plasticity of metabolic pathway flux among uropathogenic isolates of *Pseudomonas aeruginosa*. *PLoS One* 2014;9:e88368.
3. Hoffman LR, Richardson AR, Houston LS, Kulasekara HD, Martens-Habbena W *et al.* Nutrient availability as a mechanism for selection of antibiotic tolerant *Pseudomonas aeruginosa* within the CF airway. *PLoS Pathog* 2010;6:e1000712.
4. D'Argenio DA, Wu M, Hoffman LR, Kulasekara HD, Déziel E *et al.* Growth phenotypes of *Pseudomonas aeruginosa lasR* mutants adapted to the airways of cystic fibrosis patients. *Mol Microbiol* 2007;64:512–533.
5. Rohmer L, Hocquet D, Miller SI. Are pathogenic bacteria just looking for food? Metabolism and microbial pathogenesis. *Trends Microbiol* 2011;19:341–348.
6. Son MS, Matthews WJ, Kang Y, Nguyen DT, Hoang TT. *In vivo* evidence of *Pseudomonas aeruginosa* nutrient acquisition and pathogenesis in the lungs of cystic fibrosis patients. *Infect Immun* 2007;75:5313–5324.
7. Schweizer HP, Po C. Cloning and nucleotide sequence of the glpD gene encoding sn-glycerol-3-phosphate dehydrogenase of *Pseudomonas aeruginosa*. *J Bacteriol* 1994;176:2184–2193.
8. Daniels JB, Scoffield J, Woolnough JL, Silo-Suh L. Impact of glycerol-3-phosphate dehydrogenase on virulence factor production by *Pseudomonas aeruginosa*. *Can J Microbiol* 2014;60:857–863.
9. Lee SA, Gallagher LA, Thongdee M, Staudinger BJ, Lippman S *et al.* General and condition-specific essential functions of *Pseudomonas aeruginosa*. *Proc Natl Acad Sci USA* 2015;112:5189–5194.
10. Skurnik D, Roux D, Aschard H, Cattoir V, Yoder-Himes D *et al.* A comprehensive analysis of *in vitro* and *in vivo* genetic fitness of *Pseudomonas aeruginosa* using high-throughput sequencing of transposon libraries. *PLoS Pathog* 2013;9:e1003582.
11. Spoering AL, Vulic M, Lewis K. GlpD and PlsB participate in persister cell formation in *Escherichia coli*. *J Bacteriol* 2006;188:5136–5144.
12. Girgis HS, Harris K, Tavazoie S. Large mutational target size for rapid emergence of bacterial persistence. *Proc Natl Acad Sci USA* 2012;109:12740–12745.
13. Keren I, Kaldalu N, Spoering A, Wang Y, Lewis K. Persister cells and tolerance to antimicrobials. *FEMS Microbiol Lett* 2004;230:13–18.
14. Mulcahy LR, Burns JL, Lory S, Lewis K. Emergence of *Pseudomonas aeruginosa* strains producing high levels of persister cells in patients with cystic fibrosis. *J Bacteriol* 2010;192:6191–6199.
15. Luidalepp H, Jõers A, Kaldalu N, Tenson T. Age of inoculum strongly influences persister frequency and can mask effects of mutations implicated in altered persistence. *J Bacteriol* 2011;193:3598–3605.
16. Orvis J, Crabtree J, Galens K, Gussman A, Inman JM *et al.* Ergatis: a web interface and scalable software system for bioinformatics workflows. *Bioinformatics* 2010;26:1488–1492.
17. Langmead B, Trapnell C, Pop M, Salzberg SL. Ultrafast and memory-efficient alignment of short DNA sequences to the human genome. *Genome Biol* 2009;10:R25.
18. Anders S, Pyl PT, Huber W. HTSeq-a Python framework to work with high-throughput sequencing data. *Bioinformatics* 2015;31:166–169.
19. Anders S, Huber W. Differential expression analysis for sequence count data. *Genome Biol* 2010;11:R106.
20. Tatusov RL, Galperin MY, Natale DA, Koonin EV. The COG database: a tool for genome-scale analysis of protein functions and evolution. *Nucleic Acids Res* 2000;28:33–36.
21. Kanehisa M, Goto S. KEGG: kyoto encyclopedia of genes and genomes. *Nucleic Acids Res* 2000;28:27–30.
22. Livak KJ, Schmittgen TD. Analysis of relative gene expression data using real-time quantitative PCR and the 2(-Delta Delta C(T)) Method. *Methods* 2001;25:402–408.
23. Sokol PA. Production and utilization of pyochelin by clinical isolates of *Pseudomonas cepacia*. *J Clin Microbiol* 1986;23:560–562.
24. Suh SJ, Shuman J, Carroll LP, Silo-Suh L. BEEP: an assay to detect bio-energetic and envelope permeability alterations in *Pseudomonas aeruginosa*. *J Microbiol Methods* 2016;125:81–86.
25. Tabata K, Hida F, Kiriyama T, Ishizaki N, Kamachi T *et al.* Measurement of soil bacterial colony temperatures and isolation of a high heat-producing bacterium. *BMC Microbiol* 2013;13:56.
26. Cozzarelli NR, Freedberg WB, Lin EC. Genetic control of L-alpha-glycerophosphate system in *Escherichia coli*. *J Mol Biol* 1968;31:371–387.
27. Steele MI, Lorenz D, Hatter K, Park A, Sokatch JR. Characterization of the mmsAB operon of *Pseudomonas aeruginosa* PAO encoding methylmalonate-semialdehyde dehydrogenase and 3-hydroxyisobutyrate dehydrogenase. *J Biol Chem* 1992;267:13585–13592.

28. **Battesti A, Majdalani N, Gottesman S.** The RpoS-mediated general stress response in *Escherichia coli*. *Annu Rev Microbiol* 2011;65: 189–213.
29. **Kawakami T, Kuroki M, Ishii M, Igarashi Y, Arai H.** Differential expression of multiple terminal oxidases for aerobic respiration in *Pseudomonas aeruginosa*. *Environ Microbiol* 2010;12:1399–1412.
30. **Arai H, Kawakami T, Osamura T, Hirai T, Sakai Y *et al.*** Enzymatic characterization and *in vivo* function of five terminal oxidases in *Pseudomonas aeruginosa*. *J Bacteriol* 2014;196:4206–4215.
31. **Shah P, Nanduri B, Swiatlo E, Ma Y, Pendarvis K.** Polyamine biosynthesis and transport mechanisms are crucial for fitness and pathogenesis of *Streptococcus pneumoniae*. *Microbiology* 2011;157: 504–515.
32. **Bitonti AJ, McCann PP, Sjoerdsma A.** Restriction of bacterial growth by inhibition of polyamine biosynthesis by using monofluoromethylornithine, difluoromethylarginine and dicyclohexylammonium sulphate. *Biochem J* 1982;208:435–441.
33. **Lee EJ, Pontes MH, Groisman EA.** A bacterial virulence protein promotes pathogenicity by inhibiting the bacterium's own F_1F_o ATP synthase. *Cell* 2013;154:146–156.
34. **Zhang L, Alfano JR, Becker DF.** Proline metabolism increases katG expression and oxidative stress resistance in *Escherichia coli*. *J Bacteriol* 2015;197:431–440.
35. **Goncalves RL, Rothschild DE, Quinlan CL, Scott GK, Benz CC *et al.*** Sources of superoxide/H_2O_2 during mitochondrial proline oxidation. *Redox Biol* 2014;2:901–909.
36. **Prax M, Bertram R.** Metabolic aspects of bacterial persisters. *Front Cell Infect Microbiol* 2014;4:148.
37. **Radzikowski JL, Vedelaar S, Siegel D, Ortega ÁD, Schmidt A *et al.*** Bacterial persistence is an active σS stress response to metabolic flux limitation. *Mol Syst Biol* 2016;12:882.
38. **Kwan BW, Valenta JA, Benedik MJ, Wood TK.** Arrested protein synthesis increases persister-like cell formation. *Antimicrob Agents Chemother* 2013;57:1468–1473.
39. **Dörr T, Vulić M, Lewis K.** Ciprofloxacin causes persister formation by inducing the TisB toxin in *Escherichia coli*. *PLoS Biol* 2010;8: e1000317.
40. **Peterson CN, Levchenko I, Rabinowitz JD, Baker TA, Silhavy TJ.** RpoS proteolysis is controlled directly by ATP levels in *Escherichia coli*. *Genes Dev* 2012;26:548–553.
41. **Bunker JC, James AM.** Microcalorimetric studies on the effects of media and environmental conditions on the growth of bacteria. *Microbios* 1986;47:177–188.
42. **Ding L, Li X, Liu P, Li S, Lv J.** Study of the action of Se and Cu on the growth metabolism of *Escherichia coli* by microcalorimetry. *Biol Trace Elem Res* 2010;137:364–372.
43. **Russell JB.** The energy spilling reactions of bacteria and other organisms. *J Mol Microbiol Biotechnol* 2007;13:1–11.
44. **Notley L, Ferenci T.** Induction of RpoS-dependent functions in glucose-limited continuous culture: what level of nutrient limitation induces the stationary phase of *Escherichia coli*? *J Bacteriol* 1996; 178:1465–1468.
45. **Ihssen J, Egli T.** Specific growth rate and not cell density controls the general stress response in *Escherichia coli*. *Microbiology* 2004; 150:1637–1648.
46. **Battesti A, Majdalani N, Gottesman S.** Stress sigma factor RpoS degradation and translation are sensitive to the state of central metabolism. *Proc Natl Acad Sci USA* 2015;112:5159–5164.
47. **Amato SM, Fazen CH, Henry TC, Mok WW, Orman MA *et al.*** The role of metabolism in bacterial persistence. *Front Microbiol* 2014; 5:70.
48. **Shan Y, Brown Gandt A, Rowe SE, Deisinger JP, Conlon BP *et al.*** ATP-dependent persister formation in *Escherichia coli*. *MBio* 2017; 8:e02267-16–14.
49. **Meylan S, Porter CBM, Yang JH, Belenky P, Gutierrez A *et al.*** Carbon sources tune antibiotic susceptibility in *Pseudomonas aeruginosa* via tricarboxylic acid cycle control. *Cell Chem Biol* 2017;24: 195–206.
50. **Hong SH, Wang X, O'Connor HF, Benedik MJ, Wood TK.** Bacterial persistence increases as environmental fitness decreases. *Microb Biotechnol* 2012;5:509–522.
51. **Wu N, He L, Cui P, Wang W, Yuan Y *et al.*** Ranking of persister genes in the same *Escherichia coli* genetic background demonstrates varying importance of individual persister genes in tolerance to different antibiotics. *Front Microbiol* 2015;6:1003.
52. **Murakami K, Ono T, Viducic D, Kayama S, Mori M *et al.*** Role for *rpoS* gene of *Pseudomonas aeruginosa* in antibiotic tolerance. *FEMS Microbiol Lett* 2005;242:161–167.
53. **Mlynarcik P, Kolar M.** Starvation- and antibiotics-induced formation of persister cells in *Pseudomonas aeruginosa*. *Biomed Pap Med Fac Univ Palacky Olomouc Czech Repub* 2017;161.
54. **Hobby GL, Meyer K, Chaffee E.** Observations on the mechanism of action of penicillin. *Exp Biol Med* 1942;50:281–285.
55. **Dossantos RA, Alfadda A, Eto K, Kadowaki T, Silva JE.** Evidence for a compensated thermogenic defect in transgenic mice lacking the mitochondrial glycerol-3-phosphate dehydrogenase gene. *Endocrinology* 2003;144:5469–5479.
56. **Rousset S, Alves-Guerra MC, Mozo J, Miroux B, Cassard-Doulcier AM *et al.*** The biology of mitochondrial uncoupling proteins. *Diabetes* 2004;53:S130–S135.
57. **Mráček T, Drahota Z, Houštěk J.** The function and the role of the mitochondrial glycerol-3-phosphate dehydrogenase in mammalian tissues. *Biochim Biophys Acta* 2013;1827:401–410.
58. **Holloway BW, Krishnapillai V, Morgan AF.** Chromosomal genetics of *Pseudomonas*. *Microbiol Rev* 1979;43:73–102.

Edited by: M. Welch and M. Whiteley